arXiv:2206.09183v1 [cond-mat.mes-hall] 18 Jun 2022

Scaleability of dielectric susceptibility ϵ_{zz} with the number of layers and additivity of ferroelectric polarization in van der Waals semiconductors

F. Ferreira,[1,2] V. V. Enaldiev,[1,2] and V.I. Fal'ko[1,2,3]

[1] *University of Manchester, School of Physics and Astronomy, Oxford Road, Manchester M13 9PL, United Kingdom*
[2] *National Graphene Institute, University of Manchester, Booth St. E. Manchester M13 9PL, United Kingdom*
[3] *Henry Royce Institute, University of Manchester, Booth St. E. Manchester M13 9PL, United Kingdom*

We study the dielectric response of few layered crystals of various transition metal dichalcogenides (TMDs) and hexagonal Boron Nitride (hBN). We showed that the out-of-plane polarizability of a multilayer crystal (which characterizes response to the external displacement field) scales linearly with the number of layers, $\alpha_{zz}^{NL} = N\alpha_{zz}^{1L}$, independently of the stacking configuration in the film. We also established additivity of ferroelectric polarizations of consecutive interfaces in case when such interfaces have broken inversion symmetry. Then we used the obtained data of monolayer α_{zz}^{1L} to calculate the values of the dielectric susceptibilities for semiconductor TMDs and hBN bulk crystals.

I. INTRODUCTION

Dielectric permittivity is an important parameter for modeling optoelectronic devices. It characterizes how a material is polarized under an external electric field, which is relevant for modeling field-effect transistors [1, 2], capacitors [3], and ferroelectrics based memristors [4, 5]. In layered materials, dielectric permittivity reflects[6–9] a strong anisotropy of crystalline and electronic properties, which is particularly strong in van der Waals (vdW) layered crystals such as graphite, black phosphorus, hexagonal boron nitride (hBN), and transition metal dichalcogenides (TMDs). Because of the layered nature of these compounds, all of them had already been implemented as components in various field-effect transistor devices, where electrostatics is determined by the out-of-plane component of the dielectric permitivitty tensor, ϵ_{zz}. Despite its importance for device modeling, only few theoretical studies have been dedicated to the evaluation of ϵ_{zz} in layered vdW semiconductors such as InSe, GaSe, MoS_2, WS_2, $MoSe_2$, WSe_2, or $MoTe_2$, and these published[10–23] broadly disagree on their values and even qualitative dependence on the material thickness.

Here, we perform a detailed ab initio density functional theory (DFT) study of ϵ_{zz} in few-layer films of MX_2 (M=Mo,W and X=S,Se,Te) and hBN. We compute the out-of-plane polarizability, α_{zz}, of crystals with different numbers of layers and established linear scaleability of α_{zz} with the number of layers, as illustrated in Fig. 1(a). This indicates that each layer screens the external electric field independently, in agreement with other works[20, 24, 25]. In this study we take into account both electronic and ionic polarizabilities which enables us to establish the values of static and high frequency (higher than optical frequency) values of ϵ_{zz}, which appears to be particular important for hBN. We also model various stacking arrangements of layers in the multilayers, e.g., as shown in Fig 1(b), in particular those that allow for inversion symmetry broken interfaces. For such interfaces, the ferroelectric polarization is possible due to the interlayer charge transfer which also showed to be additive for consecutive interfaces.

Below, in section II, we start by discussing the DFT method which enables us to compute the values of α_{zz} for monolayers and multilayers taking into account that some of those exhibit ferroelectric interfaces. These results presented in section II demonstrate scaleability of α_{zz} in semiconducting TMDs and multilayer hBN. In section III the computed values of α_{zz} are recalculated into ϵ_{zz} of a bulk crystal which appears to be a parameter independent of the number of layers in the slab.

II. COMPUTATION OF POLARIZABILITY α_{zz}

In this work the method of choice is to compute the dependence of the energy of a thin slab of a crystal subjected to an out-of-plane displacement field using DFT. In this calculation a displacement field enters via gradient of a sawtooth potential imposed onto periodically placed few-layer 2D materials with a large spacer along z-axis. The external displacement field induces a dipole moment $\alpha_{zz}D$ which screens the displacement field inside the film and determines the material dielectric constant as it will be discussed in the next section. Here we describe the results of DFT calculations of α_{zz} for monolayer, bilayer, trilayer and tetralayer crystals from compounds listed in the introduction.

A. TMD monolayers

Here we use the approach implemented earlier in the analyses of the out-of-plane polarizability of a monolayer graphene[26]. For this we compute the total energy of a

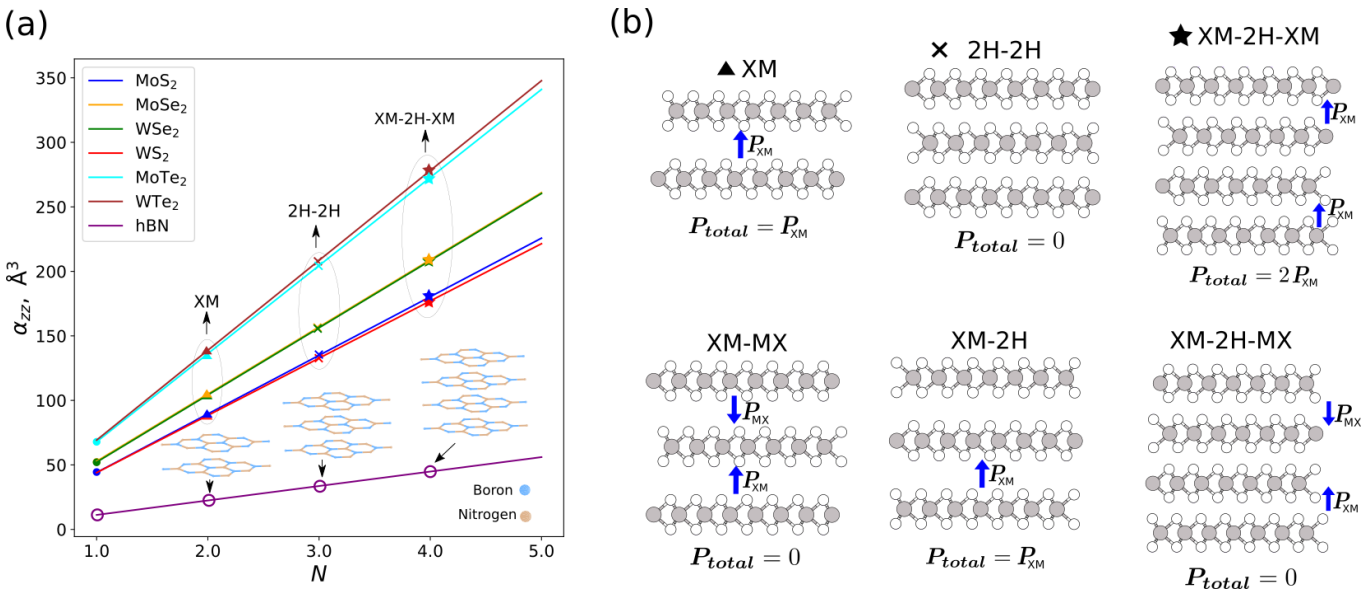


Figure 1. (a) Out-of-plane polarizability (α_{zz}) as a function of the number of layers N. Linear regressions for all materials show a coefficient of determination of $R^2 > 0.999$. Symbols correspond to values gathered from DFT calculations and lines correspond to fittings via a linear regression. The geometries that were used for multilayer TMDs in panel (a) are represented in panel (b), where it is illustrated the directions of the ferroelectric polarizations, $\boldsymbol{P}_{\rm MX}$ and $\boldsymbol{P}_{\rm XM}$, and how they contribute to the total ferroelectric polarization $\boldsymbol{P}_{total}$. Configurations used for multilayer hBN crystals can be seen in panel (a).

2D crystal per unit cell area (U) as a function of the out-of-plane displacement field (D) and fit it with a parabolic dependence[27],

$$U = U_0 - \frac{1}{2}\frac{\alpha_{zz}^{1L} D^2}{\epsilon_0 \mathcal{A}}. \quad (1)$$

Here U_0 is the energy of a unit-cell for $D = 0$, $\mathcal{A}$ is the area of the unit-cell, and ϵ_0 is the permittivity of vacuum. The DFT calculations were carried out using the plane-wave code implemented in Quantum Espresso package [28, 29]. A plane wave cut-off of 70 Ry was used for all calculations with TMDs, where the integration over the Brillouin zone was performed using the scheme proposed by Monkhorst-Pack [30] with a grid of $13 \times 13 \times 1$. We used full relativistic ultrasoft pseudopotentials with spin-orbit interaction and an exchange correlation functional that is approximated by using the PBE method [31]. The convergence threshold for self-consistency was set to 10^{-9} Ry. A Coulomb truncation[32] in the out-of-plane direction was used for all calculations and the displacement field was implemented with a z-dependent sawtooth potential. Calculations that allowed relaxation of the atomic coordinates were done using the BFGS quasi-newton algorithm, where the atoms were relaxed until the total force acting on them was smaller than 10^{-5} Ry/Bohr.

The above described DFT modeling was implemented in three ways. In one we used frozen lattice positions of all ions with spacings set to values from earlier literature[33, 34]. In the second calculation we relaxed the lattice positions of the ions for $D = 0$ imposing the lattice constant fixed to the experimentally known value without allowing further relaxation at a finite D. These two calculations returned the values of α_{zz} which can be attributed to a purely electronic response to the external perturbation which will enable us to describe the dielectric permittivity at frequencies higher than the optical phonon frequencies. In the third calculation we implemented lattice relaxation (still fixing the lateral lattice constant) for all values of D, which gives us a combined electron and ionic polarizabilities and enables us to describe static ($\omega = 0$) susceptibility of the crystal.

In Fig. 2(a), we show a typical dependence of $U(D)$ exemplified for MoS_2. To demonstrate convergence of the result against the spacing between the z-direction we show data in Fig. 2(a) for two calculations outputs: circles for an out-of-plane period of 40 Å and crosses for 70 Å. The data in Fig. 2(a) corresponds to $\alpha_{zz}^{1L} = 44.46$ Å^3. In Fig. 2(b) we show the distribution of $\Delta\rho_{zz} = \rho_{zz}^{D\neq 0} - \rho_{zz}^{D=0}$ averaged over the unit-cell of a TMD, which indicates that polarizability is dominated by the contribution of chalcogen orbitals. The values of α_{zz} computed in the above-described three ways are gathered in Table I for various TMDs. The comparison of the last two columns of Table I indicates that ionic contribution towards TMD polarizability is less than 0.2%. Therefore in the following analysis of few-layered crystals we implement the computationally less expensive first method (out of the described three), switching off lattice relaxation at all stages and using the experimentally known positions of atoms in the crystal.

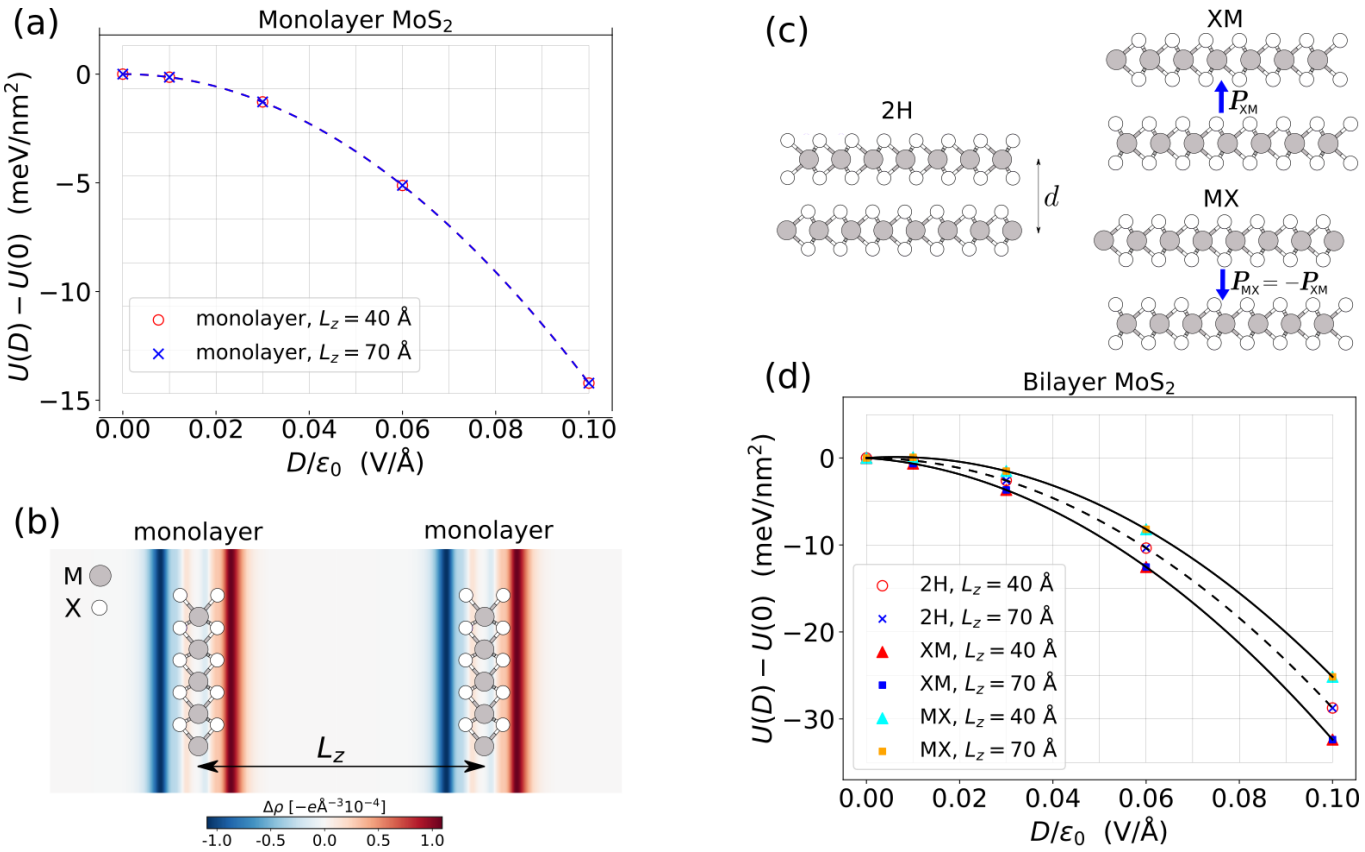


Figure 2. Total energy per unit cell area (U) of a monolayer of MoS_2 (a) and bilayer of MoS_2 with 2H-, XM- and MX-stacking configurations (b) as a function of an external out-of-plane displacement field (D). $U(0)$ is the total energy per unit cell area for a $D = 0$. Symbols represent DFT data, whereas dashed and solid lines represent the fittings to DFT data, which were computed by using the expression in Eq. (1) and (2) for monolayer and bilayers respectively. Different out-of-plane periodicities (L_z) between the crystals were used in our calculations. They are well converged at $L_z = 40$ Å for the corresponding systems. The out-of-plane averaged charge density difference for a monolayer is shown in panel (b), where blue and red regions represent the accumulation and depletion of electrons, respectively. The different stacking configurations used for our bilayer TMDs are shown in panel (c), where d is the interlayer distance and we show the directions of the ferroelectric polarization $\boldsymbol{P}_{\rm MX}$ and $\boldsymbol{P}_{\rm XM}$ due to interlayer charge transfer. The parameters obtained from our fittings are gathered in Table II.

Table I. Electronic (e) and ionic (i) contributions for the computed α_{zz} for all studied TMDs. ω_0 corresponds to the optical frequency.

	$\alpha^e_{zz}(\omega > \omega_0)$ [Å^3]	$\alpha^e_{zz}(\omega > \omega_0)$ [Å^3]	$\alpha^{e+i}_{zz}(\omega \to 0)$ [Å^3]
MoS_2	44.40	44.202	44.287
$MoSe_2$	52.295	52.646	52.646
WS_2	43.947	44.138	44.142
WSe_2	52.032	52.507	52.507
$MoTe_2$	67.897	68.050	68.232

B. TMD bilayers

In the analysis of TMD bilayers we take into account that those can be composed of qualitatively different stackings. In one, known as 2H stacking (commonly synthesized in bulk crystals) the unit cells of consecutive layers are inverted as shown in Fig. 2(c). In the other, which corresponds to stacked consecutive layers in 3R-TMD polytypes, the consecutive layers have parallel orientation of the unit cells and alignment of chalcogen atom in one layer with a metal in the other as illustrated in Fig 2(c). It has been recently shown[35–43] that such bilayers exhibit interlayer charge transfer and a spontaneous out-of-plane ferroelectric polarization with the opposite orientation for XM and MX stacking configurations (see Fig 2(c)). The results of the crystal energy computation, $U(D)$, for all of those configurations are shown in Fig. 2(d), using MoS_2 as typical example. We use such computed data to fit both spontaneous ferroelectirc polarization, P, and α_{zz} values using a parabolic dependence which now incorporates a linear term PD to account for the spontaneous interface electric dipole,

$$U - U_0 = -\frac{PD}{\epsilon_0} - \frac{1}{2}\frac{\alpha^{2L}_{zz} D^2}{\epsilon_0 \mathcal{A}}. \qquad (2)$$

The values that are extracted for the out-of-plane polarizability of MoS_2 bilayers with all the described stackings coincide (see Table II), with the DFT computation

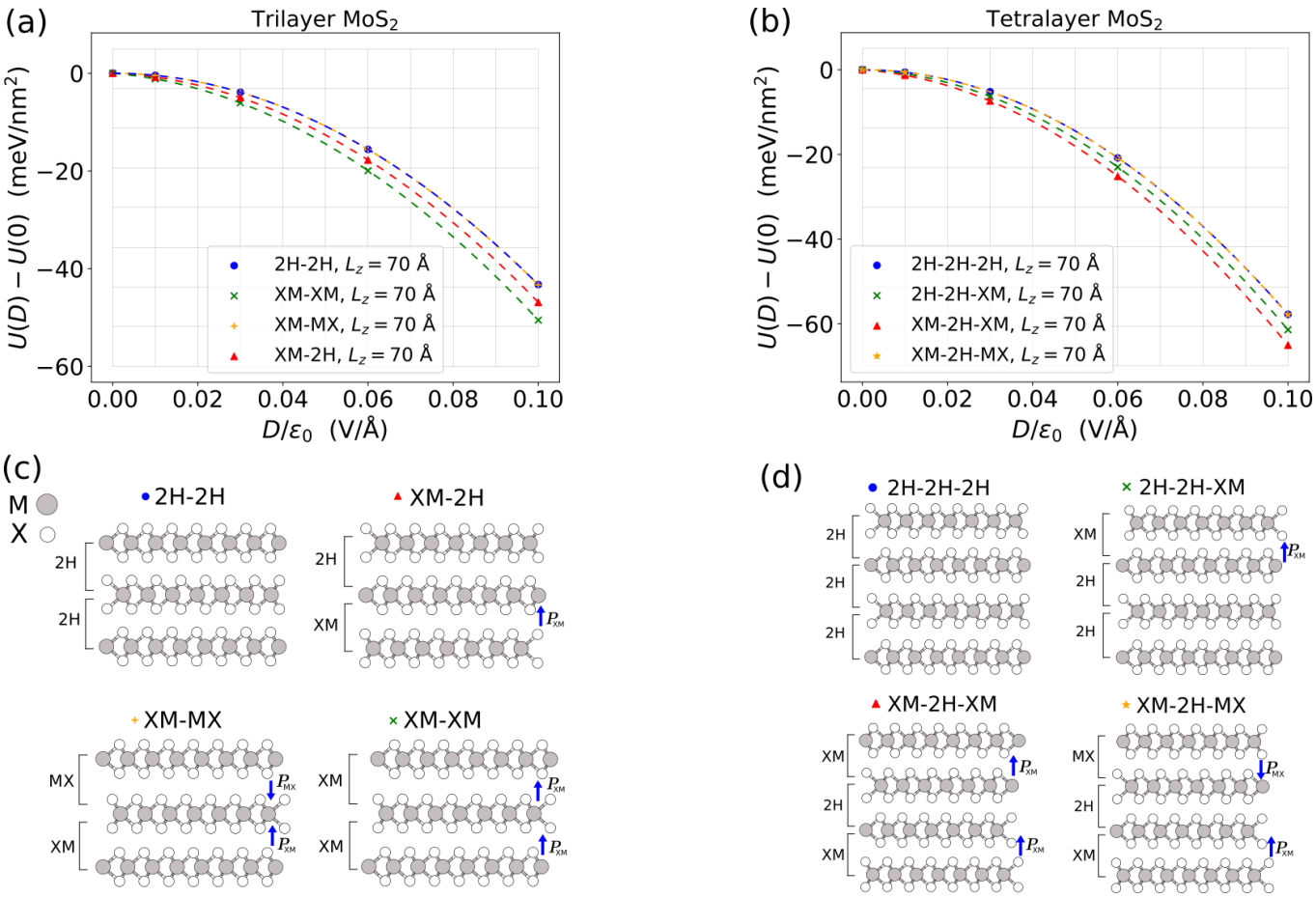


Figure 3. Total energy per unit cell area (U) of a trilayer (a) and tetralayer of MoS_2 (d) composed of different interfaces as a function of an external out-of-plane displacement field (D). Symbols represent DFT data, whereas dashed and solid lines represent the fittings to DFT data, which were computed by using the expression in Eq. (2). Our results are well converged for an out-of-plane periodicity of $L_z = 70$ Å. The interfaces used for trilayers and tetralayers TMDs are shown in panels (c) and (d) respectively and we show the directions of the ferroelectric polarization $\boldsymbol{P}_{\rm MX}$ and $\boldsymbol{P}_{\rm XM}$ due to interlayer charge transfer. The parameters obtained from our fittings are gathered in Table II.

accuracy, and appear to be approximately twice the value of monolayer polarizability. This relation between the monolayer and bilayer polarizabilities is systematically reproduced for all other four studied TMDs.

C. Trilayers and tetralayers of TMDs

To test the scaleability of α_{zz} further we considered trilayers and tetralayers with various stacking interfaces (2H-2H, XM-MX, XM-2H, XM-XM, 2H-2H-2H, XM-2H-MX, 2H-2H-XM, XM-2H-XM). The results of the DFT computed $U(D)$ depedence for each of those systems are displayed in Fig. 3(a) and (b) and analysed using Eq. (2). This produces polarizabilty values which scale linearly with the number of layers for all of those configurations as listed in Table II. The values of P obtained from the same data using Eq. (2) also correspond well to algebraic summation of independent contribution of consecutive interfaces which either compensate each other or double the resulting value (see Table II), depending on the type of interfaces in the layer stacking illustrated in Fig. 3(c) and (d). Overall the data for all five different TMDs are collected in Fig.1(a) where one can see that $\alpha_{zz}^{NL} = N\alpha_{zz}^{1L}$, where N is the number of layers.

D. Monolayer and multi-layer hBN crystals

In this subsection we repeat the analysis of α_{zz} for hexagonal boron nitride crystals, this includes the study of lattice relaxation and ionic contribution towards polarizability and additivity of ferroelectric polarization due to the interlayer charge transfer in inversion-asymmetric interfaces. We carried out DFT calculations using the plane-wave code implemented in Quantum Espresso package [28, 29]. A plane wave cut-off of 90 Ry was used for all calculations with hBN films, where the integration over the Brillouin zone was performed using the scheme proposed by Monkhorst-Pack [30] with a

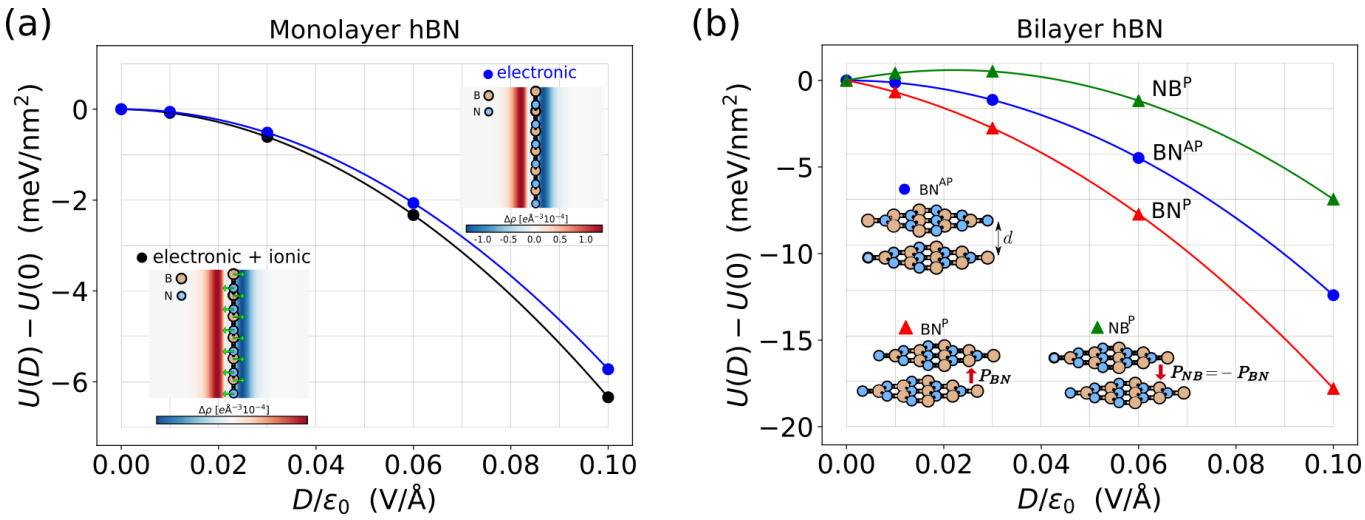


Figure 4. Total energy per unit cell area (U) of a monolayer of hBN (a) and bilayer of hBN with BN^{AP}, BN^{P} and NB^{P}-stacking configurations (b) as a function of an external out-of-plane displacement field (D). $U(0)$ is the total energy per unit cell area for a $D = 0$. Symbols represent DFT data, whereas solid lines represent the fittings to DFT data, which were computed by using the expression in Eq. (1). The out-of-plane averaged charge density difference $\Delta\rho$ for a monolayer is shown as an inset in (a), where blue and red regions represent the accumulation and depletion of electrons, respectively. The different stacking configurations used for our bilayers of hBN are shown in (b), where d is the interlayer distance and we show the directions of the ferroelectric polarization $\boldsymbol{P}_{\rm NB}$ and $\boldsymbol{P}_{\rm BN}$ due to interlayer charge transfer. The parameters obtained from our fittings are gathered in Table III.

Table II. Values of P and α_{zz} obtained by fitting DFT data to Eq. (1) and (2) for monolayer and multilayer MoS_2 crystals respectively. In the second column we indicate the interfaces that contribute to the ferroelectric prolarization (FP) of each crystal (see Fig. 1 and 2). In the fifth column we show the ratio between α_{zz} and α_{zz}^{1L}, where the latter corresponds to α_{zz} of a monolayer.

MoS_2	FP interfaces	P $10^{-4}e/$Å	α_{zz} Å^3	$\alpha_{zz}/\alpha_{zz}^{1L}$
monolayer	-	0	44.40	1.00
2H	-	0	88.81	2.00
MX	$\boldsymbol{P}_{\rm MX}$	-3.6	88.91	2.00
XM	$\boldsymbol{P}_{\rm XM}$	3.6	88.89	2.00
2H-2H	-	0	135.16	3.04
XM-MX	$\boldsymbol{P}_{\rm XM} + \boldsymbol{P}_{\rm MX}$	0	135.33	3.05
XM-2H	$\boldsymbol{P}_{\rm XM}$	3.7	135.24	3.05
XM-XM	$2\boldsymbol{P}_{\rm XM}$	7.3	135.32	3.05
2H-2H-2H	-	0	180.50	4.07
XM-2H-MX	$\boldsymbol{P}_{\rm XM} + \boldsymbol{P}_{\rm MX}$	0	180.56	4.07
2H-2H-XM	$\boldsymbol{P}_{\rm XM}$	3.7	180.57	4.07
XM-2H-XM	$2\boldsymbol{P}_{\rm XM}$	7.3	180.67	4.07

grid of $9 \times 9 \times 1$. For hBN calculations, we used norm conserving pseudopotentials and an exchange correlation functional that is approximated by using the PBE method[31], with the inclusion of a van-der-Waals functional described by Tkatchenko–Scheffler vdW-TS[44]. The convergence threshold for self-consistency was set to 10^{-9} Ry. A z-dependent sawtooth potential was used to induce an out-of-plane displacement field where an out-of-plane Coulomb truncation [32] was considered. Relaxation calculations for the atomic coordinates were done using the BFGS quasi-newton algorithm, with a threshold convergence for the total force acting on the atoms less than 10^{-5} Ry/Bohr

In contrast to TMDs the out-of-plane relaxation of ions (for a lattice constant fixed to the experimentally known value) gives two clearly distinguishable $U(D)$ dependence which result in the values of α_{zz}^{e} and α_{zz}^{e+i} listed in Table III. An example of calculations for three stacking configurations of hBN bilayers (with parallel and anti-parallel unit cell orientations), performed with lattice relaxation implemented in the code, are displayed in Fig. 4(b). The difference between the $U(D)$ dependence results from the ferroelectric polarization of bilayers with parallel unit cells orientations[40, 41, 43, 45]. The values of α_{zz}^{e+i} for these bilayers as well for trilayers and tetralayers listed in Table III demonstrate perfect scaleability with the number of layers, $\alpha_{zz}^{NL} = N\alpha_{zz}^{1L}$, for both electronic and combined electronic plus ionic responses. Moreover, ferroelectric polarization exhibits additivity of contribution of individual interfaces.

III. DISCUSSION

In order to recalculate the computed α_{zz} into dielectric constant of a medium composed of many layers in a TMD or hBN crystal, we use the following expression

$$\epsilon_{zz} = \left(1 - \frac{\alpha_{zz}^{1L}}{\mathcal{A}d}\right)^{-1}. \qquad (3)$$

Table III. Values of P and α_{zz} obtained by fitting DFT data to Eq. (1) for monolayer (1L) and multi-layer (2L, 3L, 4L) hBN crystals respectively. In the second column we indicate the interfaces that contribute to the ferroelectric prolarization (FP) of each crystal (see Fig. 4). In the sixth and ninth column we show the ratio between α_{zz} and α_{zz}^{1L} with and without ionic contribution.

			Electronic (e)			Electronic (e) + ionic (i)		
hBN		FP interfaces	P $10^{-4}e/$Å	α_{zz}^{e} Å^3	$\alpha_{zz}^{e}/\alpha_{zz}^{1L(e)}$	P $10^{-4}e/$Å	α_{zz}^{e+i} Å^3	$\alpha_{zz}^{e+i}/\alpha_{zz}^{1L(e+i)}$
1L		-	0	11.20	1.00	0	12.07	1.00
2L	BN^{AP}	-	0	22.56	2.01	0	24.23	2.01
	BN^{P}	$\boldsymbol{P}_{BN}$	5.8	22.46	2.01	5.5	24.09	2.00
	NB^{P}	$\boldsymbol{P}_{NB}$	-5.7	22.47	2.01	-5.4	24.09	2.00
3L	BN^{AP}-BN^{AP}	-	0	33.88	3.02	0	36.32	3.01
	BN^{P}-NB^{P}	$\boldsymbol{P}_{\rm BN}+\boldsymbol{P}_{\rm NB}$	0	33.67	3.01	0	36.03	2.99
	BN^{P}-BN^{P}	$2\boldsymbol{P}_{\rm BN}$	12.0	33.69	3.01	11.7	36.19	3.00
4L	BN^{AP}-BN^{AP}-BN^{AP}	-	0	45.17	4.03	0	48.73	4.04
	BN^{P}-NB^{P}-BN^{P}	$2\boldsymbol{P}_{\rm BN}+\boldsymbol{P}_{\rm NB}$	5.9	44.88	4.01	6.3	49.05	4.06
	BN^{P}-BN^{P}-BN^{P}	$3\boldsymbol{P}_{\rm BN}$	17.5	44.86	4.01	17.9	48.48	4.02

Table IV. Dielectric constant ϵ_{zz} of bulk TMDs studied in this work and hBN, monolayer band gap E_g^{1L}, monolayer out-of-plane polarizabilites α_{zz}^{1L}. For the latter we show the value calculated here, theoretical values from other works that carried out DFPT (density functional perturbation theory) calculations, other theoretical methods different from DFPT and measured values obtained experimentally.

	This work	DFPT	Other methods	Measured	E_g^{1L} [eV]	α_{zz} [Å^3]
ϵ^{MoS_2}	6.10	7.6[17], 6.87[21], 6.9[23]	3.92[15], 6.3[20], 10.08[22]	4.9[12], 3.7[16][a], 6.2[11]	1.71	44.47
ϵ^{WS_2}	5.84	6.87[17], 6.4[23]	5.14[15], 6.0[20], 6.39[22]		1.67	43.95
ϵ^{MoSe_2}	7.34	8.5[23]	6.07[15],7.8[20]		1.41	52.29
ϵ^{WSe_2}	7.20	7.8[23]	5.16[15],7.7[20]		1.33	52.03
ϵ^{MoTe_2}	10.69	16.10[15]	10.4[23]		1.02	67.91
$\epsilon^{hBN}_{(\omega>\omega_0)}$	2.64	3.38 [13], 3.57[14], 5.09[19], 3.76[23]	2.7[20]	5.09 [10], 3.5-3.8[46], 3 to 5[18])	4.62	11.24
$\epsilon^{hBN}_{(\omega\to0)}$	3.00	2.84 [13], 2.95[14], 3.61[19], 3.03[23]		4.10 [10]	4.62	12.07

[a] Layer with a thickness of 30 nm.

which has been successfully implemented before in the analyses of layered materials[25, 26, 39]. In Table IV we gather the resulting values of ϵ_{zz} (obtained from the corresponding computed values of α_{zz}^{1L}) for all the materials studied here). As we found in section II that for TMDs the ionic contribution is negligibly small, the results of ϵ_{zz} are expected to be the same for both zero and high frequencies. For hBN the low and high frequency dielectric constants are distinguishable due to a substantial contribution of ions towards static polarizability evident in Table IV. Nevertheless the overall dielectric constant of hBN is smaller than of TMDs due to a weaker electronic polarizabilty which we attribute to a much larger band gap of this material.

IV. CONCLUSIONS

The analysis presented here demonstrates linear scaling of polarizability of multilayer TMDs and hBN with the number of layers of these van der Waals materials which suggests that layers respond to the out-of-plane perturbation independently of each other. This enabled us to quantify the dielectric constant of these materials determined by such polarizabilty of the layers with the values of the computed polarizabilities that we compare with the results of previous computations and some experimentally available data in Table IV.

ACKNOWLEDGMENTS

This work was supported by EC-FET European Graphene Flagship Core3 Project, EC-FET Quantum Flagship Project 2D-SIPC, EPSRC grants EP/S030719/1 and EP/V007033/1, and the Lloyd Register Foundation Nanotechnology Grant. Computational resources were provided by the Computational Shared Facility of the University of Manchester and the ARCHER2 UK National Supercomputing Service (https://www.archer2.ac.uk) through EPSRC Access to HPC project e672.

[1] A. Younis, J. Alsaei, B. Al-Najar, H. Manaa, P. Rajan, E. H. S. Sadki, A. Loucif, and S. Sehar, Recent advances in functional 2D materials for field effect transistors and nonvolatile resistive memories, in *2D Functional Nanomaterials* (John Wiley and Sons, Ltd, 2021) Chap. 10, pp. 175–198.

[2] A. Sebastian, R. Pendurthi, T. H. Choudhury, J. M. Redwing, and S. Das, Benchmarking monolayer MoS_2 and WS_2 field-effect transistors, Nature Communications **12**, 693 (2021).

[3] Poonam, K. Sharma, A. Arora, and S. Tripathi, Review of supercapacitors: Materials and devices, Journal of Energy Storage **21**, 801 (2019).

[4] T. Mikolajick, S. Slesazeck, H. Mulaosmanovic, M. H. Park, S. Fichtner, P. D. Lomenzo, M. Hoffmann, and U. Schroeder, Next generation ferroelectric materials for semiconductor process integration and their applications, Journal of Applied Physics **129**, 100901 (2021).

[5] A. Weston, E. G. Castanon, V. Enaldiev, F. Ferreira, S. Bhattacharjee, S. Xu, H. Corte-León, Z. Wu, N. Clark, A. Summerfield, T. Hashimoto, Y. Gao, W. Wang, M. Hamer, H. Read, L. Fumagalli, A. V. Kretinin, S. J. Haigh, O. Kazakova, A. K. Geim, V. I. Fal'ko, and R. Gorbachev, Interfacial ferroelectricity in marginally twisted 2d semiconductors, Nature Nanotechnology **17**, 390 (2022).

[6] F. Hüser, T. Olsen, and K. S. Thygesen, How dielectric screening in two-dimensional crystals affects the convergence of excited-state calculations: Monolayer MoS_2, Phys. Rev. B **88**, 245309 (2013).

[7] S. Latini, T. Olsen, and K. S. Thygesen, Excitons in van der Waals heterostructures: The important role of dielectric screening, Phys. Rev. B **92**, 245123 (2015).

[8] F. Ferreira, A. J. Chaves, N. M. R. Peres, and R. M. Ribeiro, Excitons in hexagonal boron nitride single-layer: a new platform for polaritonics in the ultraviolet, J. Opt. Soc. Am. B **36**, 674 (2019).

[9] A. Ceferino, K. W. Song, S. J. Magorrian, V. Zólyomi, and V. I. Fal'ko, Crossover from weakly indirect to direct excitons in atomically thin films of InSe, Phys. Rev. B **101**, 245432 (2020).

[10] R. Geick, C. H. Perry, and G. Rupprecht, Normal modes in hexagonal boron nitride, Phys. Rev. **146**, 543 (1966).

[11] T. J. Wieting and J. L. Verble, Infrared and raman studies of long-wavelength optical phonons in hexagonal mos_2, Phys. Rev. B **3**, 4286 (1971).

[12] R. A. Neville and B. L. Evans, The band edge excitons in 2H-MoS_2, physica status solidi (b) **73**, 597 (1976).

[13] N. Ohba, K. Miwa, N. Nagasako, and A. Fukumoto, First-principles study on structural, dielectric, and dynamical properties for three BN polytypes, Phys. Rev. B **63**, 115207 (2001).

[14] Y. Cai, L. Zhang, Q. Zeng, L. Cheng, and Y. Xu, Infrared reflectance spectrum of BN calculated from first principles, Solid State Communications **141**, 262 (2007).

[15] R. K. Ghosh and S. Mahapatra, Monolayer transition metal dichalcogenide channel-based tunnel transistor, IEEE Journal of the Electron Devices Society **1**, 175 (2013).

[16] C.-P. Lu, G. Li, K. Watanabe, T. Taniguchi, and E. Y. Andrei, MoS_2: Choice substrate for accessing and tuning the electronic properties of graphene, Phys. Rev. Lett. **113**, 156804 (2014).

[17] L. Liang and V. Meunier, First-principles Raman spectra of MoS_2, WS_2 and their heterostructures, Nanoscale **6**, 5394 (2014).

[18] S. M. Kim, A. Hsu, M. H. Park, S. H. Chae, S. J. Yun, J. S. Lee, D.-H. Cho, W. Fang, C. Lee, T. Palacios, M. Dresselhaus, K. K. Kim, Y. H. Lee, and J. Kong, Synthesis of large-area multilayer hexagonal boron nitride for high material performance, Nature Communications **6**, 8662 (2015).

[19] L. Wang, Y. Pu, A. K. Soh, Y. Shi, and S. Liu, Layers dependent dielectric properties of two dimensional hexagonal boron nitridenanosheets, AIP Advances **6**, 125126 (2016).

[20] J. Koo, S. Gao, H. Lee, and L. Yang, Vertical dielectric screening of few-layer van der Waals semiconductors, Nanoscale **9**, 14540 (2017).

[21] N. A. Pike, A. Dewandre, B. Van Troeye, X. Gonze, and M. J. Verstraete, Vibrational and dielectric properties of the bulk transition metal dichalcogenides, Phys. Rev. Materials **2**, 063608 (2018).

[22] M. Farkous, M. Bikerouin, H. T. T. Phung, M. El-Yadri, E. Feddi, F. Dujardin, C. A. Duque, D. Muoi, H. V. Phuc, C. V. Nguyen, and N. N. Hieu, Electronic and optical properties of layered van der Waals heterostructure based on MS_2 (M = Mo, W) monolayers, Materials Research Express **6**, 065060 (2019).

[23] A. Laturia, M. L. Van de Put, and W. G. Vandenberghe, Dielectric properties of hexagonal boron nitride and transition metal dichalcogenides: from monolayer to bulk, npj 2D Materials and Applications **4**, 28 (2020).

[24] E. K. Yu, D. A. Stewart, and S. Tiwari, Ab initio study of polarizability and induced charge densities in multilayer graphene films, Phys. Rev. B **77**, 195406 (2008).

[25] T. Tian, D. Scullion, D. Hughes, L. H. Li, C.-J. Shih, J. Coleman, M. Chhowalla, and E. J. G. Santos, Electronic polarizability as the fundamental variable in the dielectric properties of two-dimensional materials, Nano Letters **20**, 841 (2020).

[26] S. Slizovskiy, A. Garcia-Ruiz, A. I. Berdyugin, N. Xin, T. Taniguchi, K. Watanabe, A. K. Geim, N. D. Drummond, and V. I. Fal'ko, Out-of-plane dielectric susceptibility of graphene in twistronic and bernal bilayers, Nano Letters **21**, 6678 (2021).

[27] Z. Adamczyk, Chapter 2 - potential interactions among particles, in *Particles at Interfaces*, Interface Science and Technology, Vol. 20, edited by Z. Adamczyk (Elsevier, 2017) pp. 9–167.

[28] P. Giannozzi, S. Baroni, N. Bonini, M. Calandra, R. Car, C. Cavazzoni, D. Ceresoli, G. L. Chiarotti, M. Cococcioni, I. Dabo, A. D. Corso, S. de Gironcoli, S. Fabris, G. Fratesi, R. Gebauer, U. Gerstmann, C. Gougoussis, A. Kokalj, M. Lazzeri, L. Martin-Samos, N. Marzari, F. Mauri, R. Mazzarello, S. Paolini, A. Pasquarello, L. Paulatto, C. Sbraccia, S. Scandolo, G. Sclauzero, A. P. Seitsonen, A. Smogunov, P. Umari, and R. M. Wentzcovitch, QUANTUM ESPRESSO: a modular and open-source software project for quantum simulations of materials, Journal of Physics: Condensed Matter **21**, 395502 (2009).

[29] P. Giannozzi, O. Andreussi, T. Brumme, O. Bunau, M. B. Nardelli, M. Calandra, R. Car, C. Cavazzoni, D. Ceresoli, M. Cococcioni, N. Colonna, I. Carnimeo, A. D. Corso, S. de Gironcoli, P. Delugas, R. A. DiStasio, A. Ferretti, A. Floris, G. Fratesi, G. Fugallo, R. Gebauer, U. Gerstmann, F. Giustino, T. Gorni, J. Jia, M. Kawamura, H.-Y. Ko, A. Kokalj, E. Küçükbenli, M. Lazzeri, M. Marsili, N. Marzari, F. Mauri, N. L. Nguyen, H.-V. Nguyen, A. O. de-la Roza, L. Paulatto, S. Poncé, D. Rocca, R. Sabatini, B. Santra, M. Schlipf, A. P. Seitsonen, A. Smogunov, I. Timrov, T. Thonhauser, P. Umari, N. Vast, X. Wu, and S. Baroni, Advanced capabilities for materials modelling with quantum ESPRESSO, Journal of Physics: Condensed Matter **29**, 465901 (2017).

[30] H. J. Monkhorst and J. D. Pack, Special points for brillouin-zone integrations, Phys. Rev. B **13**, 5188 (1976).

[31] J. P. Perdew and A. Zunger, Self-interaction correction to density-functional approximations for many-electron systems, Phys. Rev. B **23**, 5048 (1981).

[32] T. Sohier, M. Calandra, and F. Mauri, Density functional perturbation theory for gated two-dimensional heterostructures: Theoretical developments and application to flexural phonons in graphene, Phys. Rev. B **96**, 075448 (2017).

[33] W. Schutte, J. De Boer, and F. Jellinek, Crystal structures of tungsten disulfide and diselenide, Journal of Solid State Chemistry **70**, 207 (1987).

[34] K. Bronsema, J. De Boer, and F. Jellinek, On the structure of molybdenum diselenide and disulfide, Zeitschrift für Anorganische und Allgemeine Chemie **540**, 15 (1986).

[35] A. Weston, Y. Zou, V. Enaldiev, A. Summerfield, N. Clark, V. Zólyomi, A. Graham, C. Yelgel, S. Magorrian, M. Zhou, J. Zultak, D. Hopkinson, A. Barinov, T. H. Bointon, A. Kretinin, N. R. Wilson, P. H. Beton, V. I. Fal'ko, S. J. Haigh, and R. Gorbachev, Atomic reconstruction in twisted bilayers of transition metal dichalcogenides, Nature Nanotechnology **15**, 592 (2020).

[36] F. Ferreira, V. V. Enaldiev, V. I. Fal'ko, and S. J. Magorrian, Weak ferroelectric charge transfer in layer-asymmetric bilayers of 2D semiconductors, Scientific Reports **11**, 13422 (2021).

[37] V. V. Enaldiev, F. Ferreira, S. J. Magorrian, and V. I. Fal'ko, Piezoelectric networks and ferroelectric domains in twistronic superlattices in WS_2/MoS_2 and $WSe_2/MoSe_2$ bilayers, 2D Materials **8**, 025030 (2021).

[38] S. J. Magorrian, V. V. Enaldiev, V. Zólyomi, F. Ferreira, V. I. Fal'ko, and D. A. Ruiz-Tijerina, Multifaceted moiré superlattice physics in twisted WSe_2 bilayers, Phys. Rev. B **104**, 125440 (2021).

[39] V. V. Enaldiev, F. Ferreira, and V. I. Fal'ko, A scalable network model for electrically tunable ferroelectric domain structure in twistronic bilayers of two-dimensional semiconductors, Nano Letters 10.1021/acs.nanolett.1c04210 (2022).

[40] L. Li and M. Wu, Binary compound bilayer and multilayer with vertical polarizations: Two-dimensional ferroelectrics, multiferroics, and nanogenerators, ACS Nano **11**, 6382 (2017).

[41] C. R. Woods, P. Ares, H. Nevison-Andrews, M. J. Holwill, R. Fabregas, F. Guinea, A. K. Geim, K. S. Novoselov, N. R. Walet, and L. Fumagalli, Charge-polarized interfacial superlattices in marginally twisted hexagonal boron nitride, Nature Communications **12**, 347 (2021).

[42] N. R. Walet and F. Guinea, Flat bands, strains, and charge distribution in twisted bilayer $h-$BN, Phys. Rev. B **103**, 125427 (2021).

[43] K. Yasuda, X. Wang, K. Watanabe, T. Taniguchi, and P. Jarillo-Herrero, Stacking-engineered ferroelectricity in bilayer boron nitride, Science **372**, 1458 (2021).

[44] A. Tkatchenko and M. Scheffler, Accurate molecular van der waals interactions from ground-state electron density and free-atom reference data, Phys. Rev. Lett. **102**, 073005 (2009).

[45] N. R. Walet and F. Guinea, Flat bands, strains, and charge distribution in twisted bilayer $h-$BN, Phys. Rev. B **103**, 125427 (2021).

[46] F. Ahmed, S. Heo, Z. Yang, F. Ali, C. H. Ra, H.-I. Lee, T. Taniguchi, J. Hone, B. H. Lee, and W. J. Yoo, Dielectric dispersion and high field response of multilayer hexagonal boron nitride, Advanced Functional Materials **28**, 1804235 (2018).